Max-Planck-Institut für Meteorologie

Report No. 11

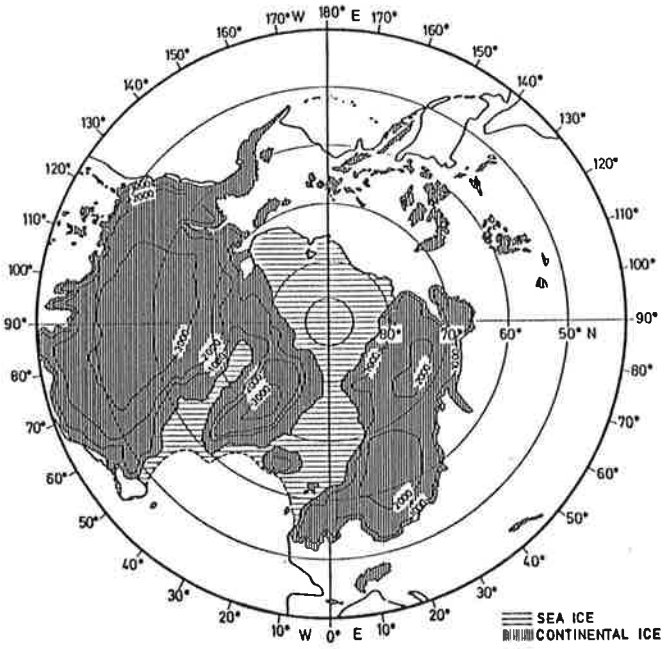

SIMULATION OF THE JANUARY CLIMATE 18000 YBP

by

MICHAEL LAUTENSCHLAGER · KLAUS HERTERICH

ULRICH SCHLESE · EDILBERT KIRK

HAMBURG, SEPTEMBER 1987

AUTHORS:

MICHAEL LAUTENSCHLAGER — MAX-PLANCK-INSTITUT FÜR METEOROLOGIE

KLAUS HERTERICH — MAX-PLANCK-INSTITUT FÜR METEOROLOGIE

ULRICH SCHLESE — METEOROLOGISCHES INSTITUT DER UNIVERSITÄT HAMBURG
BUNDESSTRASSE 55
D - 2000 HAMBURG 13

EDILBERT KIRK — METEOROLOGISCHES INSTITUT DER UNIVERSITÄT HAMBURG
BUNDESSTRASSE 55
D - 2000 HAMBURG 13

MAX-PLANCK-INSTITUT
FÜR METEOROLOGIE
BUNDESSTRASSE 55
D-2000 HAMBURG 13
F.R. GERMANY

Tel.: (040) 41 14 - 1
Telex: 211092
Telemail: K. Hasselmann
Telefax: (040)4114-298

Simulation of the January Climate 18000 YBP

M. Lautenschlager, K. Herterich

Max-Planck-Institut für Meteorologie, Hamburg

U. Schlese, E. Kirk

Meteorologisches Institut der Universität Hamburg

Contents

1. Introduction

Information about the climate of the earth's past (paleoclimate) may help to understand climate dynamics at long time scales, i.e thousands or millions of years. Parts of the earth climate development is recorded in e.g. ocean sediments. Today available sediment cores include climate information of the last million years. On one side these information is restricted to some quantities, e.g. sea surface temperature, global ice volume and sea ice extention , on the other side it is applicable at the geographical core location only. If it is wanted to extend the core information mathematical modeling based on physical reasoning must be applied. Paleoclimatic simulations are interesting as attempt to understand the earth history and as model tests which give hints about model reliability.

In paleoclimatic modeling two strategies are followed up to learn something about the earth climate and its development. The method of time series modelling produces long time series with highly paramterized mathematical models. A model hypothesis e.g. the global ice volume dependence on the insolation variation of the sun is tested against the core records of the global ice volume. This report is engaged in the second method . The method of time slice modeling produces global model climates at certain times with threedimensional , primitive equation models. The models based on a simple set of mathematical statements which are assumed to be rooted in the conservation laws of mass, momentum and energy.

Under the present available computer facilities and the state of art in climate modeling only the calculation of climatic states in the subsystems,land, ice, ocean and atmosphere, of the coupled global climatic system is possible. The conditions of the unconsidered subsystems must be prescribed as boundary conditions for

e.g. the atmosphere.Comparing two different time slices something can be learned about the behaviour of the considered subsystem under different boundary conditions if it is assumed that the used model represents reality.

During the past 18.000 years the climatic state changed from full glaciation to interglacial conditions. The last glacial maximum is located in time at 18000 years before present (YBP). (Last ice age: 8000 YBP - 70000 YBP, Würm- or Weichsel ice age.) The climate state is characterized by large ice sheets which covered parts of North-America, Europe and Asia. Grounded ice lay over the whole antarctic continental shelf and the today typical shelf ice regions (swimming ice areas of some hundert meter thickness) vanished. Sea ice in both hemispheres extended 10° latitude or more further equatorward than at present. The atmosphere was cooler and drier in comparison with the present climate.

The underlying questions of this report are:
What is the global distribution of the January climate 18000 YBP of the atmosphere under prescribed land, ice and ocean conditions and what are the differences compared with a January climate simulation at present?
Answering these questions the T21 version of the ECMWF spectral GCM (general circulation model) is used.

The second section of this report specifies the boundary condition changes for the paleo-run (18000 YBP). The third section presents the model results, while in the fourth section a signal-to-noise analysis is performed to answer the question whether the simulated paleo-and control-climate are significantly different or not. The fifth and sixth section deal with comparisons with observations and recent simulation results, while in the last section a short summary is presented.

2. T21-Model and Boundary Conditions

The T21-model is a spectral model for the adiabatic calculations. Definition of boundary values at the earth surface and parameterization of physical processes are done on a 64 x 32 grid. The spectral resolution of the T21-model is up to wave number 21. The horizontal grid is divided into 32 latitude points ($\Delta \simeq 5.6°$) and 64 longitude points ($\Delta \simeq 5.6°$). The vertical direction is separated into 16 levels in hybrid σ-p coordinates. Beside the calculation of wind, temperature, pressure and humidity, turbulence, radiation, convection and precipitation are included in the model in parameterized form. The surface temperature and - moisture over land is calculated by a 3 layer soil model. For further information about the T21- model see Louis (1984) and Dümenil, Schlese (1987a).

Two simulation experiments are performed with the T21-model (Cycle 24):

paleo - experiment: the January climate at the last ice age maximum (18000 YBP),

control - experiment: the January climate at present (0 YBP).

The following model input must be changed from modern- to January - 18000 YBP - conditions to carry out the paleo - experiment.

Parameters:

a) orbit parameters

b) ozon distribution

c) CO_2 - concentration

d) areosol concentration

e) radiation

Boundary conditions:

f) sea - land - distribution

g) orography

h) sea- surface - temperature

i) surface albedo

j) deep soil temperature

k) deep soil moisture

a) orbit parameters:

The elliptical orbit of the earth around the sun is characterized by three parameters: eccentricity, axial tilt and position of perihelion. The used values are taken from Kutzbach, Guetter (1986) and are summarized in table 1.

Table 1: orbit parameters

	Eccentricity of orbit	Axial tilt (degrees)	Position of perihelion (*) (degrees)
0 YBP	0.0167	23.44	78
18000 YBP	0.0195	23.45	16.3

((*) measured clockwise from vernal equinox)

The eccentricity is a measure of the deviation of the earth's orbit from a cycle. 18000 YBP the orbit is a little more elliptical than today. The axial tilt measures the angle between the earth's rotation axis and the normal of the earth's orbit around the sun. The position of the perihelion gives the point in the earth's orbit nearest the sun. Today the perihelion is about 1st January, 18000 YBP it is about 8th March. The altered orbit parameters lead to a decrease of insolation of about 1% for January 18000 YBP.

b) ozon distribution:

No information about the ozon distribution 18000 YBP is available. So the actual distribution is used for the paleo- simulation, too.

c) CO_2-concentration:

The atmospheric CO_2 concentration is reduced from 330 ppm in the control run to 200 ppm for the paleo experiment in agreement with Kutzbach, Guetter (1986).

d) aerosol concentration:

One type of aerosol is used. The concentration depends on height only. The modern concentration is applied to the paleo-experiment in absence of information about aerosol concentration 18000 YBP.

e) radiation:

The radiation input is set to the 15th January and held constant.

f) sea - land - distribution:

The distinction between ocean and land is necessary because the model physics in both types of points is different. Fig. 2.1 shows the input-masks and gives an impression of the model resolution (64 longitude and 32 latitude points) and of the distribution of ice, sea and land. The masks are built up from the ice age information of CLIMAP (1981). The sea ice points are considered as water with very low temperature (about 30°C under freezing level).

g) orography:

The orography enters the T21-model as grid point heights and surface roughness. In each surface grid area the mean height (H) and the mountain height, characterized by h_m, is determined. Land point heights are determined after the atlas of Diercke (1968), ice elevation after CLIMAP (1981). For 18000

YBP a sea level reduction of 100 m and glaciation of the Himalaya after Kuhle (1986) are included. The surface roughness (z_o) is determined after Rotta (1972) to include mountain drag effects:

$$z_o = \Delta_h \, e^{-\kappa \cdot C}$$

where

$\Delta_h = h_m - H$: height difference in grid area,

$K = 0.41$: von Karman constant,

$C = 12$: empirical constant for about 5% of the grid area covered with mountains of the height h_m.

For sea-ice a surface roughness of $z_0 = 0.001$m is taken. The z_o - values of ocean points are computed after the Charnock-formula (Louis (1984)).

h) sea-surface-temperature (SST):

The SST is determined as a grid area average of the values given by CLIMAP (1981).

i) surface albedo:

In agreement with the T21-model the surface albedo of land-ice, sea-ice and ocean is set to:

$A_L = 0.8$ (land-ice, snow),

$A_S = 0.55$ (sea-ice),

$A = 0.07$ (ocean).

The surface albedo of the land-points is determined as a grid area average of the values given by CLIMAP (1981). Ten albedo classes between $A^* = 0.1$ and $A^* = 0.5$ are specified.

j) deep soil temperature and

k) deep soil moisture

The surface temperature and moisture at land points are calculated in the T21-model including a three-layer soil model. The soil model needs the moisture and temperature climate in 70 cm soil depth as boundary values. These deep soil values are assumed to be constant during one month. They are estimated from the present values under consideration of general climate information 18000 YBP (about 5°C colder and drier than today) and the surface albedo to distinct different soil and vegetation classes.

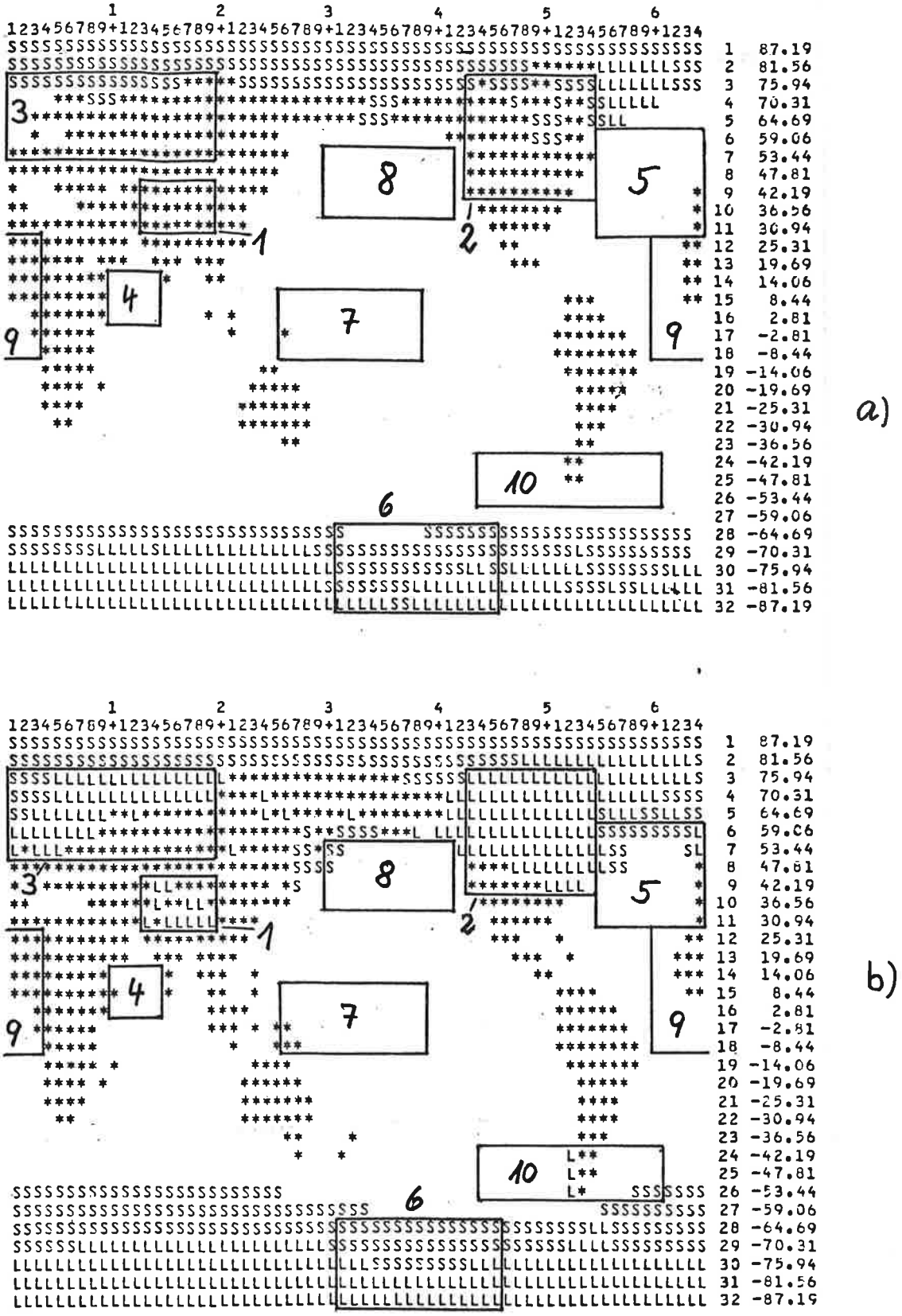

Figure 2.1: Sea-land-mask of the T21-model
a) Control - experiment
b) Paleo - experiment
(Symbols: L - land-ice, S - sea-ice, * - land, blank - sea;
Boxes 1-10: Statistical test pattern for signal-to-noise analysis)

3. Climate Means and Anomalies

The experiments (paleo and control) are set up as perpetual January runs with the T21-model and the boundary conditions described in section 2. 16 January months are calculated in each run. The shown results are the mean over the last 12 monthly means and are designated as climate means. The climate means are fairly free of monthly fluctuations because of averaging.

So far only surface values are evaluated because they can be compared with results of other simulation experiments and datas resulting from analyses of ocean sediments and land deposits. The following quantities are plotted as paleo-climate (January 18000 YBP), control-climate (January 0 YBP) and the anomaly of paleo- and control-climate:

- deviation of the reduced surface pressure (sea level) from global mean (fig. 3.1)
- surface wind (fig. 3.2)
- surface temperature (fig. 3.3)
- precipitation (fig. 3.4)
- snow fall (fig. 3.5)
- evaporation (fig. 3.6)

The pressure reduced to sea level is an artificial quantity and includes two effects, a vertical extrapolation effect and the "true" climate effect connected with the atmospheric circulation, we are mainly interested in. The vertical extrapolation differences in the two experiments due to changes in orographic heights and in vertical temperature gradients near the surface will be obvious in different global surface pressure means:

- paleo global mean: 1021 HPA
- control global mean: 1007 HPA

The extrapolation effects are dropped at least partly if the pressure deviation from the global mean (fig.3.1) is considered. If the pressure anomalies are considered the surface pressure anomalies correspond with the surface wind anomalies. Both experiments show similar structures in the pressure distribution in the northern hemisphere. The increase of pressure over the additional land and sea ice in the paleo-experiment appears reasonable in terms of surface cooling. The decrease of sea level pressure over the Antarctican is not in accord with this simple-minded argument.

The differences in the pressure deviation (fig.3.1) between the paleo- and control-climate correspond with the surface wind anomalies (fig.3 2). In the paleo-climate the easterly trade in the Pacific is reduced and the intertropical convergence zone near Africa over the Atlantic is about 10° more in the south. The winds down the Himalaya to the Arabean Sea, which are responsible for the winter monsoon, are intensified. In the southern hemisphere and over the ice sheets the wind acitvity is enlarged.

The surface temperature (fig.3.3) over land is in general 5°C - 10°C smaller in the paleo climate than in the control run except Alaska and Central -Asia, where a temperature increase of about 5°C is observed. The temperature increase in Alaska corresponds with the intensification of the North-Pacific low, while the reason for a temperature increase over Central Asia is not obvious. In the Sahara the surface temperature is reduced by an amount of 10°C to 15°C in the paleo-experiment. In the central region of the Sahara where mountains are located, the model produces surface temperatures below 0°C for January 18000 YBP.

The precipitation (fig.3.4) and evaporation (fig.3.6) is in general increased over ocean areas and decreased over land in the paleo climate, which agress with only minor changes in the sea surface temperature and the stronger cooling of the

land surface. Especially the winter monsoon around India and the precipitation in the Northern Pacific and -Atlantic and in the tropical area of the Eastern Atlantic and Pacific is enlarged.

The snow fall (fig.3.5), part of the precipitation, is concentrated along the ice edges and increases in the paleo-climate especially in the northern hemisphere.

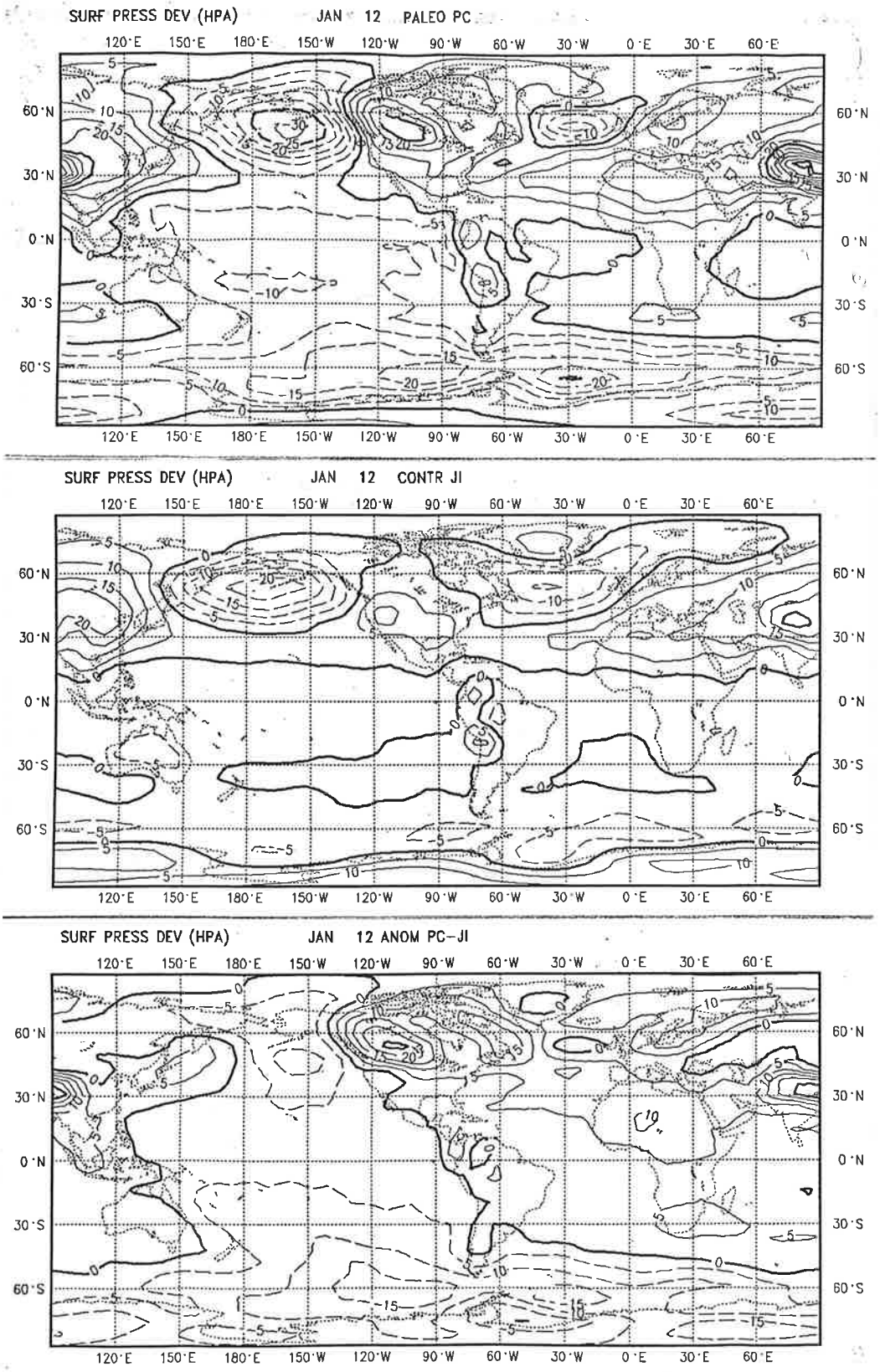

Figure 3.1: Deviation of reduced surface pressure from global mean (paleo global mean: 1021 HPA, control global mean: 1007 HPA)

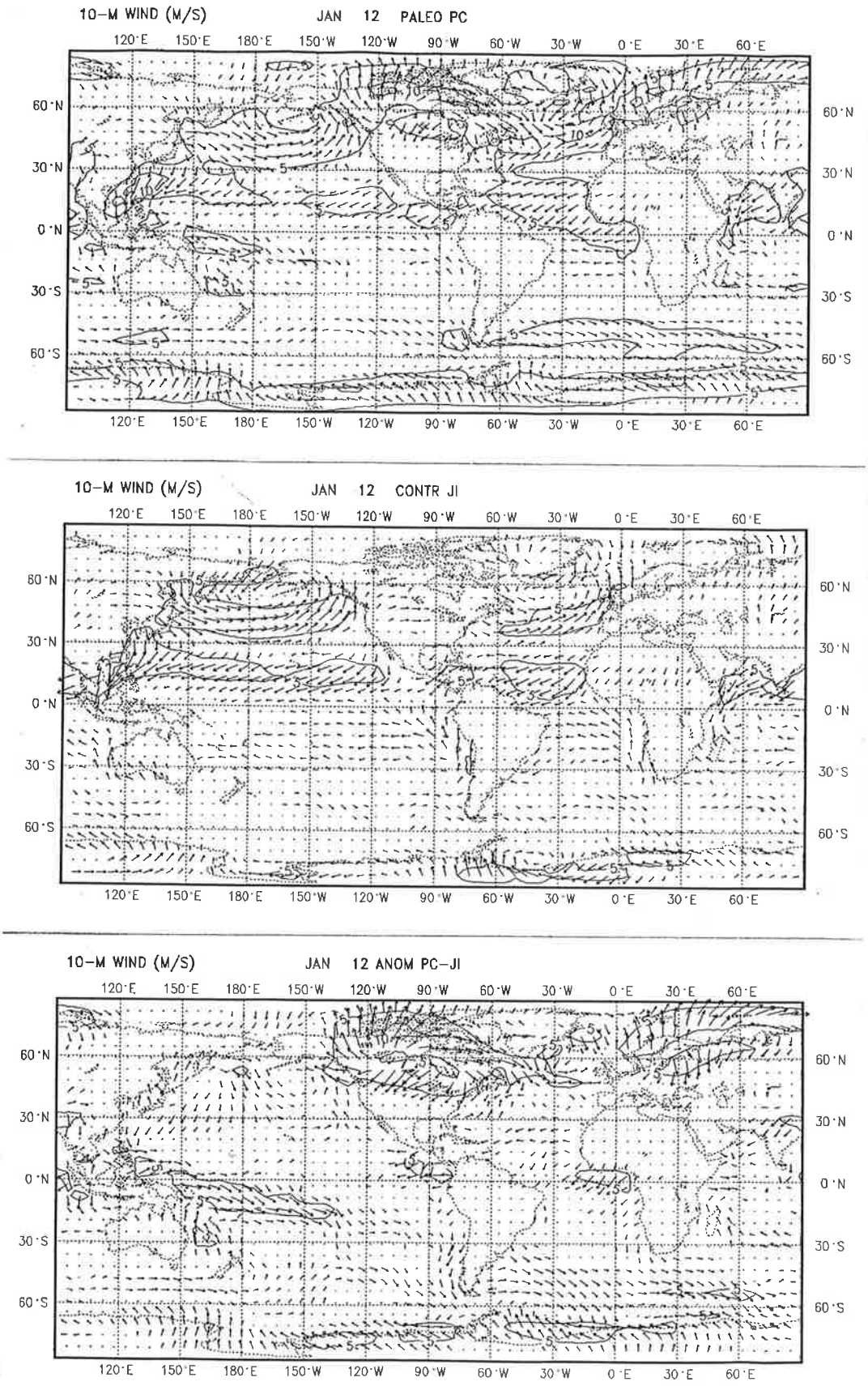

Figure 3.2: Surface wind in m/s

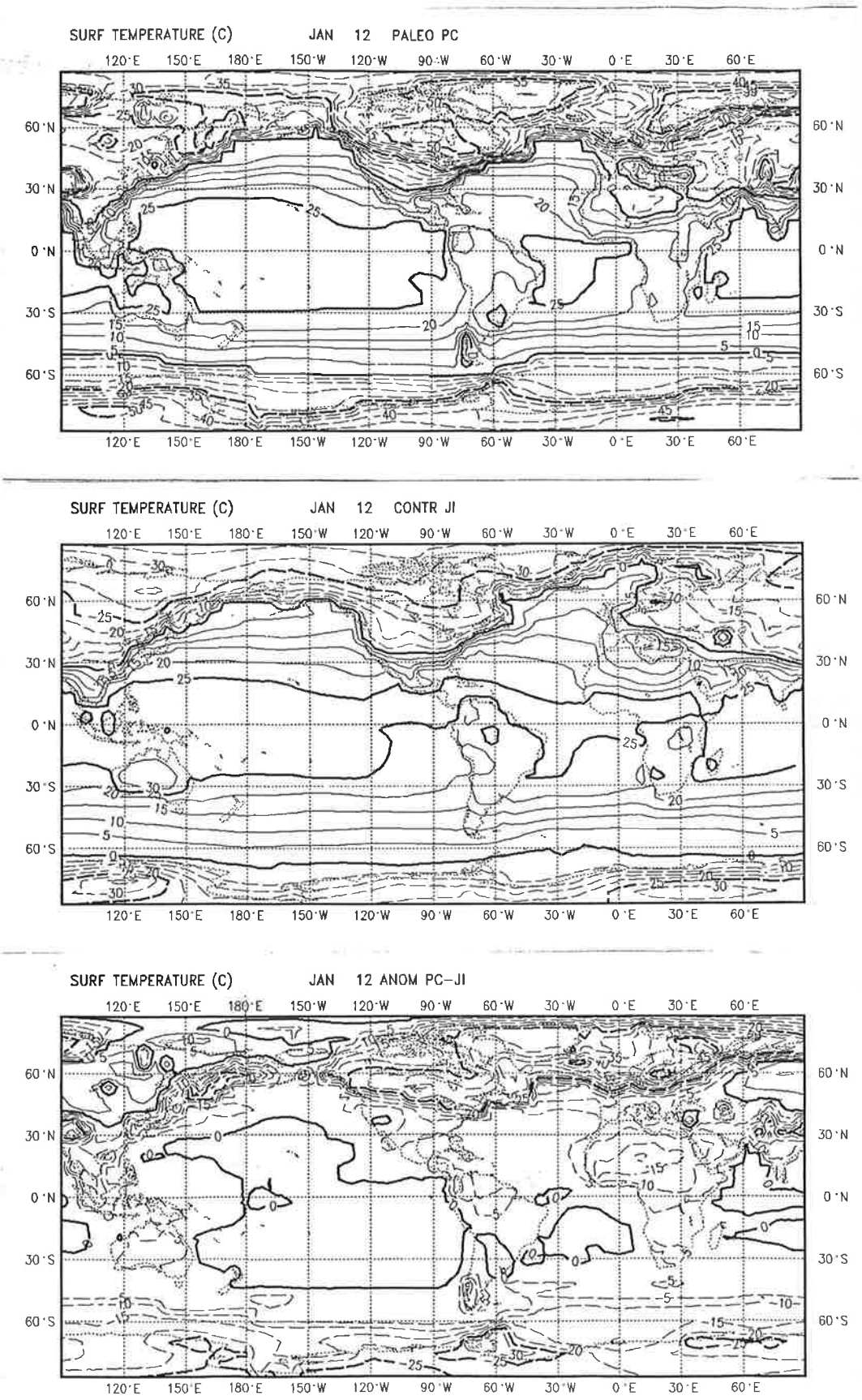

Figure 3.3: Surface temperature in °C

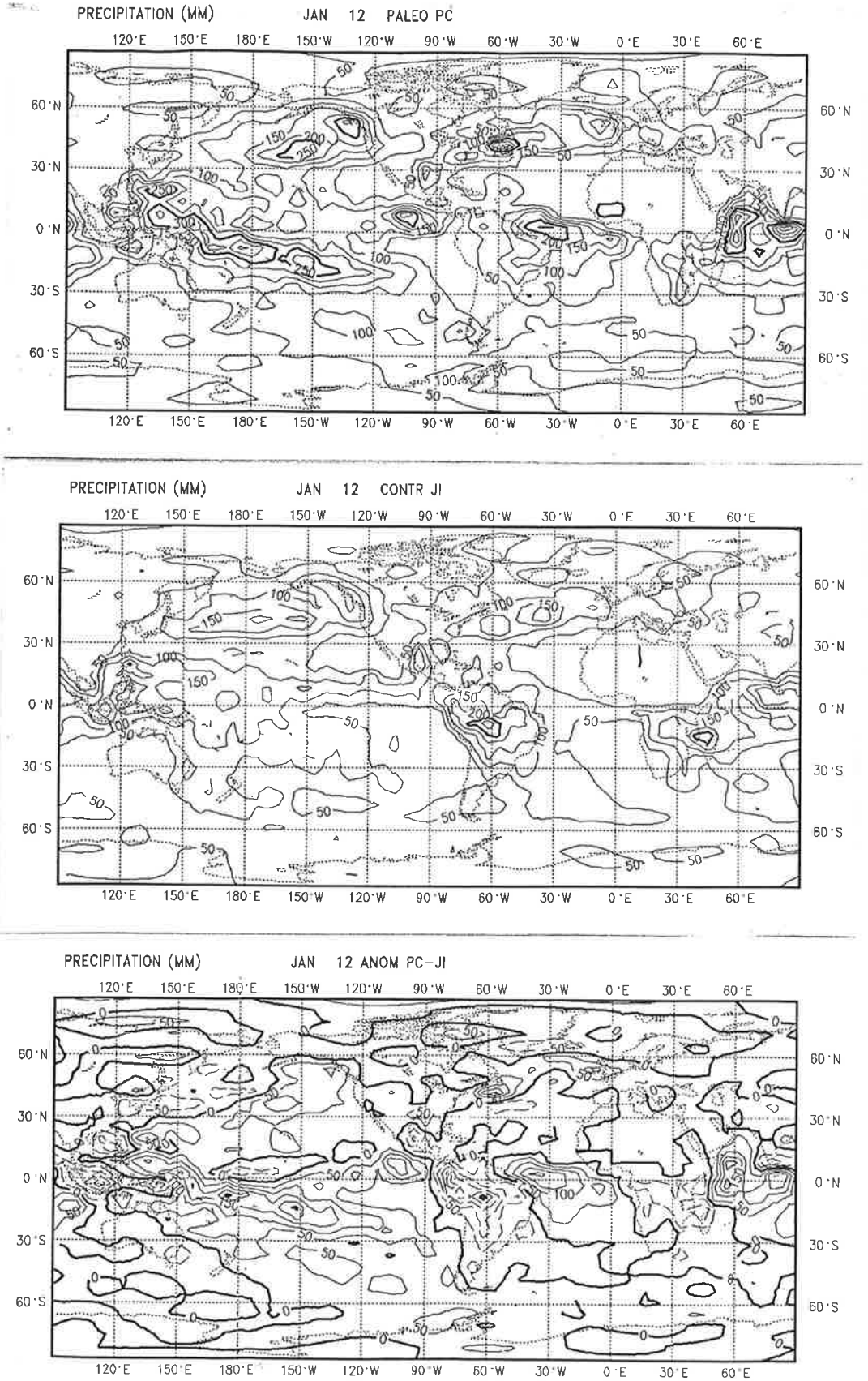

Figure 3.4: Precipitation (monthly mean in mm-water equivalent)

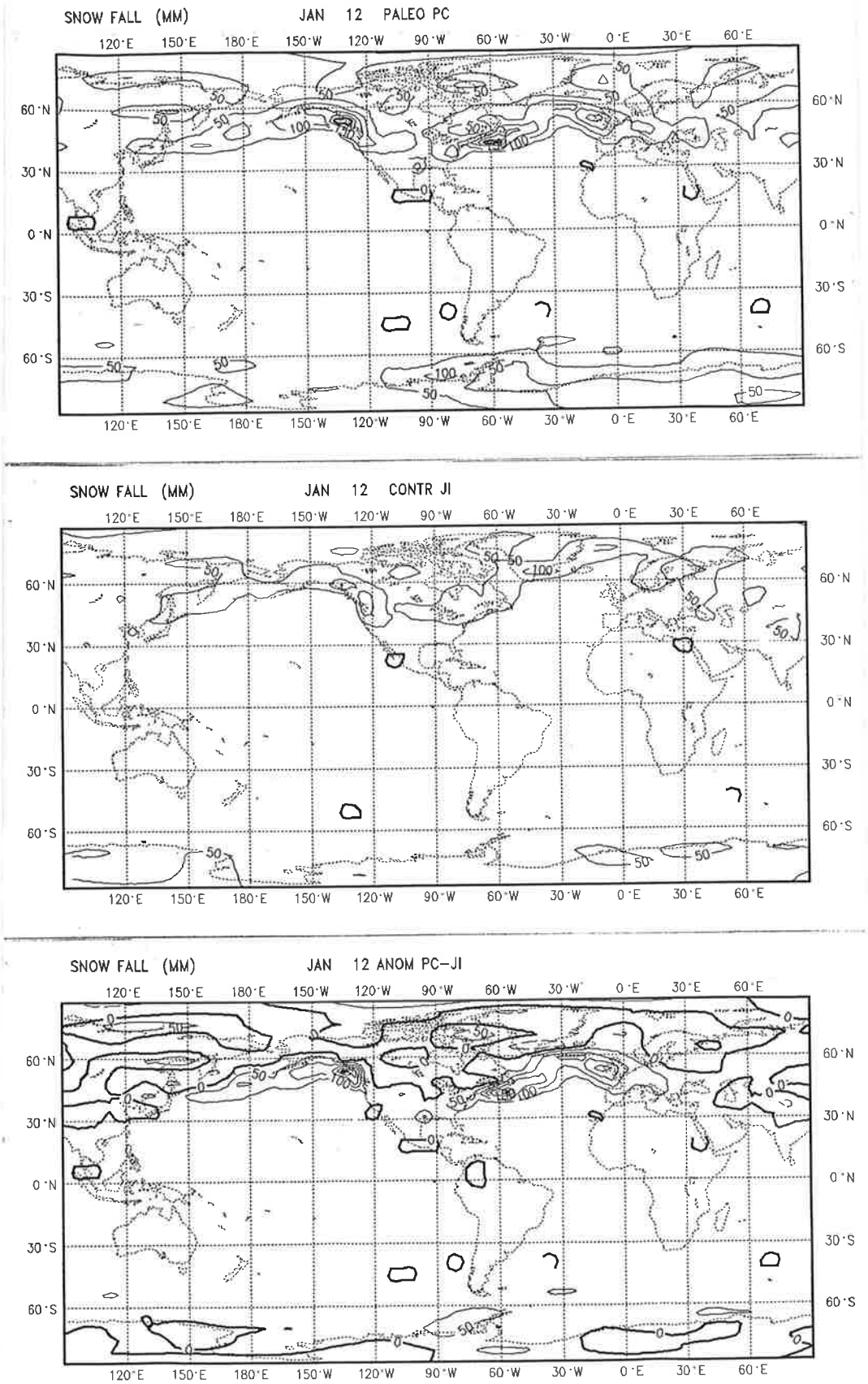

Figure 3.5: Snowfall (monthly mean in mm-water equivalent)

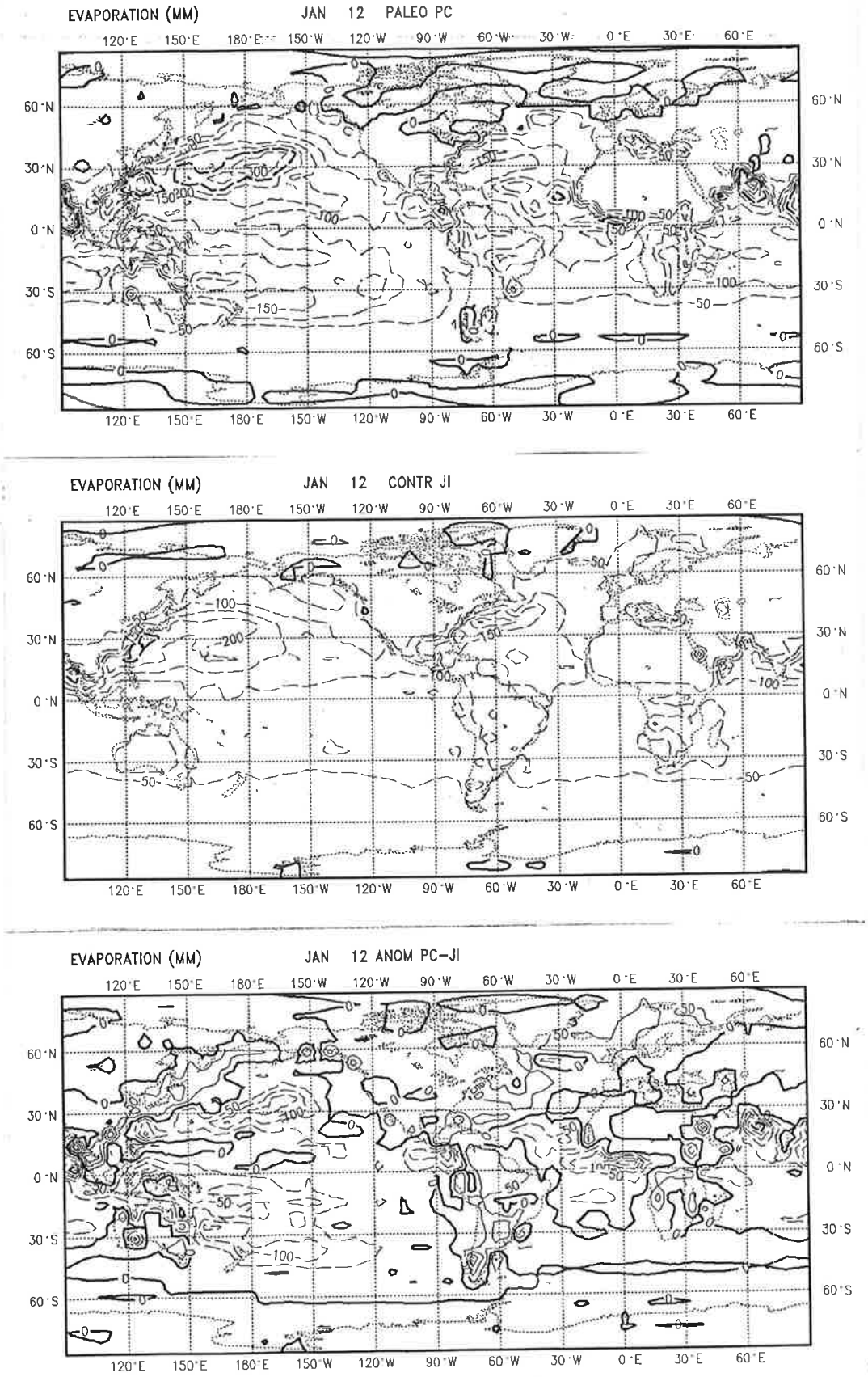

Figure 3.6: Evaporation (monthly mean in mm-water equivlaent)

4. Signal-to noise Analysis

A statistical analysis is performed to answer two questions:

1) Are the global climatic states in the control - and the paleo-experiment significantly different?

2) Where are great climatic influences located?

Looking at the global fields in fig. 3.1 - fig. 3.6 the answer of the first question is 'yes' with great probability while the answer of the second question is not obvious.

The datas resulting from perpetual January runs are given as grid point values in a field size of 64x32 = 2048 points. For each experiment, control and paleo, twelve monthly mean fields are evaluated.

The simplest possibility of statistical analysis is a univariate test where a quantity is tested independently point by point. A commonly used test of this kind is the t-test (see Hannoschöck, Frankignoul (1985)). The random variable t is proportional to the difference of the control - and the anomaly (here: paleo) mean scaled by the variance square root at each grid point. The univariate t-test leads to local information only and the criterion whether global fields are different or not is unclear.

The strong spatial interdependence of atmsopheric data points is considered in multivariate tests where the whole global fields are tested against each other. The test is here performed as the Hotelling T^2 - test (for detailed information see Hannoschöck, Frankignoul (1985), Hannoschöck (1984)). The test hypothesis is the so called null hypothesis. The Hotelling test answers the question: 'Are the global fields of a specific quantity in the control and anomaly experiment equal?'

including a specific risk with

- yes, they are, or
- no, they are not.

The null hypothesis can be tested for a quantity x by considering the T^2 - statistic:

$$T^2 = \left(\frac{1}{N} + \frac{1}{M} \right)^{-1} (x^a - x^c)^T S^{-1} (x^a - x^c),$$

where

x^a: n_p-dimensional vector averaged over the M realizations of the anomaly (paleo) experiment,

x^c: n_p-dimensional vector averaged over the N realizations of the control experiment (global field site $n_p = 2048$)

$(x^a - x^c)$: deviation vector of estimated means,

$(x^a - x^c)^T$: transposed deviation vector,

S^{-1}: inverse of an unbiased estimate of the true error covariance matrix equal in both experiments.

The (n_p x n_p) - matrix S will be estimated from the experimental data. Discrete Fourier amplitudes are computed from all available experiment realizations (control and anomaly). The cut-off frequency in the estimation of S is given by the condition that the square of the Fourier amplitudes are approximately constant in the intervall $O < f_k \leq f_{nf}$. The condition guarantees the unbiased estimate of S. Here the first four frequencies ($n_f = 4$) are taken. The frequency f_4 corresponds with a period of 1.5 months which can be interpreted as the minimum time seperation of independent atmospheric phenomena. The error

covariance matrix is the density of the cross spectrum at frequency f_k = O and is a real quantity. (see Hannoschöck (1984)).

The cut-off frequency f_4 leads to an upper limit to the degrees of freedom and therefore to the dimension of the matrix S. Eight frequencies, four in the control and four in the anomaly experiment, are used to estimate the matrix S. Each frequency consists of a real and an imaginary part, which are uncorrelated random variables. So the upper limit to the degrees of freedom follows as

$$n = 2 \cdot 2 \cdot 4 = 16.$$

The null-hypothesis is rejected at a certain α-level (risk) if

$$T^2 > \frac{(N+M-2)n}{N+M-n-1} F(\alpha; n, N+M-n-1)$$

where F(α; n, N + M - n- 1) is the Fischer's F-distribution (see e.g. Aramowitz, Stegun (1968)).

The global fields of the model data must be compressed because of the limitation in the degrees of freedom: $n_{global} = 2048 >> n_{limit} = 16$. The data reduction is performed by choosing ten a priori test patterns (see fig. 2.1). The choice is motivated by the location of the glacial ice sheets and the general known atmospheric phenomena during the last ice age. The area means of the test patterns enter the Hotelling T^2 - test.

The standard deviation is calculated for the area means of each test pattern and for different quantities. The maximum values of the standard deviations are

summarized in table 2. The standard deviations are of the same order of magnitude which give hints about the same month-to-month variability in the paleo and the present climate produced by the T21-model.

Table 2: maximum standard deviations of the test pattern area means

	paleo	control
surface pressure (HPA)	4	5
surface temperature (°C)	0.9	0.8
precipitation (mm)	18	15
total surface wind (m/s)	1.0	1.5
zonal surface wind (m/s)	0.8	1.3
meridional surface wind (m/s)	0.6	0.7

The multivariate statistical test is performed with the program package 'SNAP' ('signal-to-noise analysis program' by G. Hannoschöck, H. Kruse, T. Bruns). The test variables are in this first approach:

- sea level pressure (fig 4.1)
- surface temperature (fig 4.2)
- precipitation (fig. 4.3)
- zonal surface wind (fig. 4.4)
- meridional surface wind (fig. 4.5)

An impression of the different statistical weight of the single test patterns is given due to a test hierarchy which is specified by the a priori numbering of the

test patterns. The test hierarchy is built up by running the T^2-test ten times with the pattern partial sums:

1.: pattern 1

2.: pattern 1 + 2

3.: pattern 1 + 2 + 3

.

.

.

10.: pattern 1 + 2 + 3 + ... + 10

The partial sums are indicated in fig. 4.1 - fig. 4.5 as 'number of parameters'.

All five tested variables show the climate state in the paleo experiment is significantly different from the climate in the control experiment. In all cases the significance is greater than 99.9%. The Himalaya pattern (1) alone locates the significance above the 99.9% - curve. (The pattern numbers are given in the brackets and scetched in fig. 2.1).

Beside the Himalaya (1) a few other patterns exist which are responsible for a further increase in significance:

- sea level pressure: North American ice sheet (2)
- surface temperature: North-American - (2), Eurasian ice sheet (3), Antarctic (6)
- precipitation: Arabian Sea (4), equatorial Pacific (7), west coast of Africa (9)
- zonal surface wind: equatorial Pacific (7)
- meridional surface wind equatorial Pacific (7), North Pacific (8), west coast of Africa (9)

The results of the statistical tests are the climate state of the ice age is different from the present climate while the variability is in both cases the same, and the glaciation of the Himalaya is of great importance in the ice age climate. The individual importance of the patterns will be clearer if the given pattern hierarchy is altered in a way that patterns are tested alone and/or dropped from the given hierarchy. A further extention of the statistical test to global fields of variables in the upper atmosphere is planned.

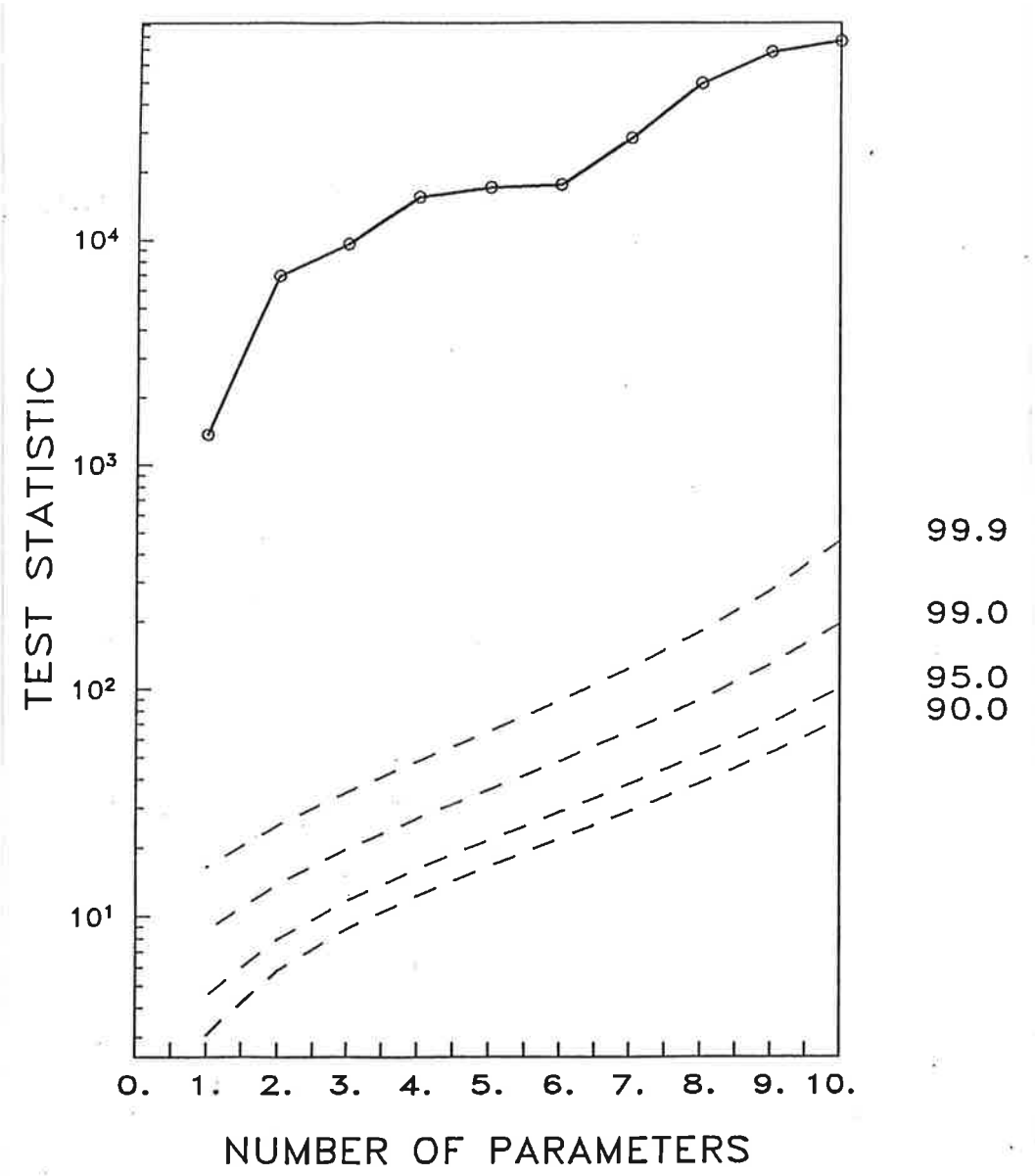

Figure 4.1: Hotelling T^2 -test of sea level pressure, axis' number of parameters': partial sums in test hierarchy

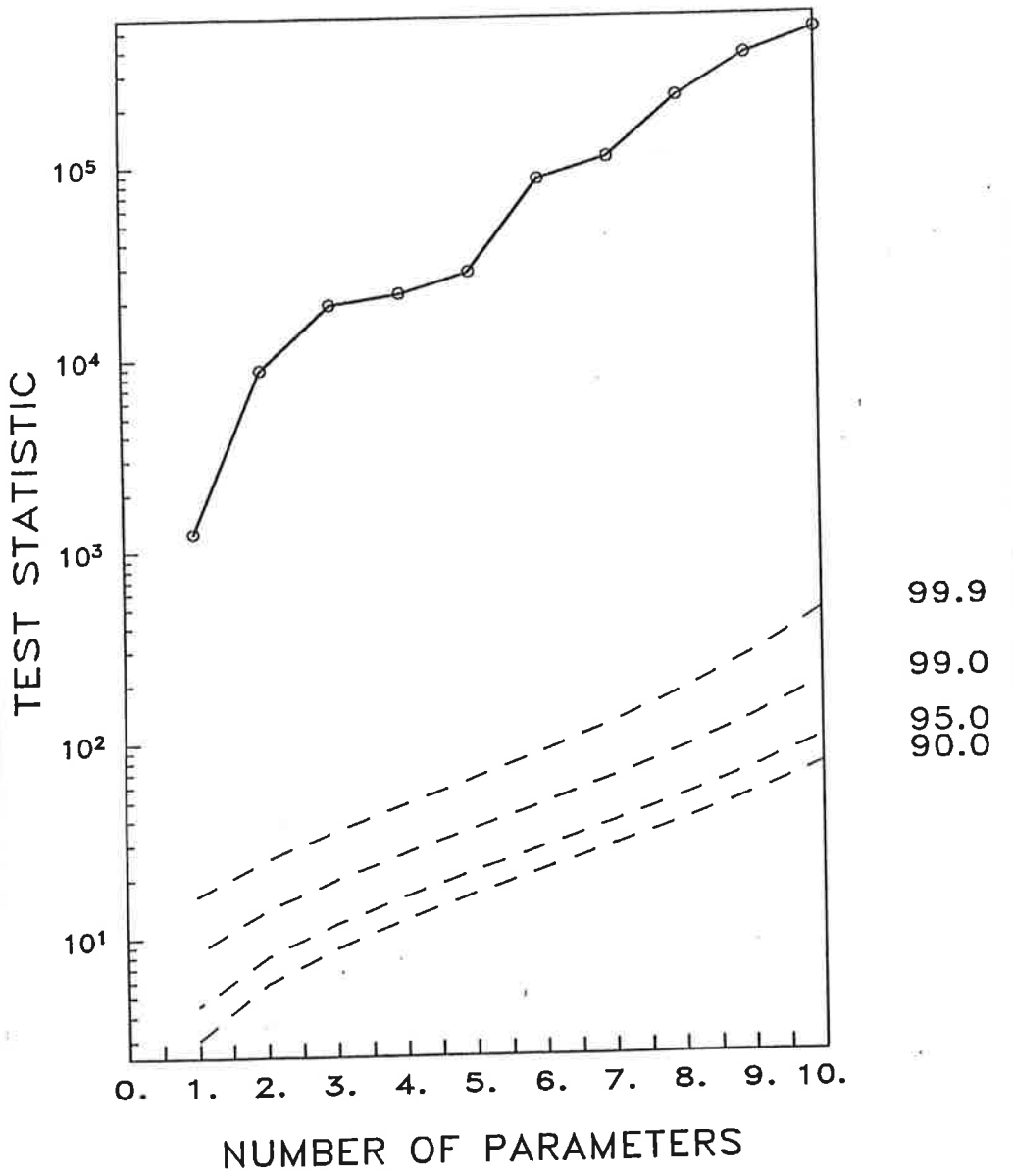

Figure 4.2: Hotelling T^2 - test of surface temperature, axis see fig. 4.1

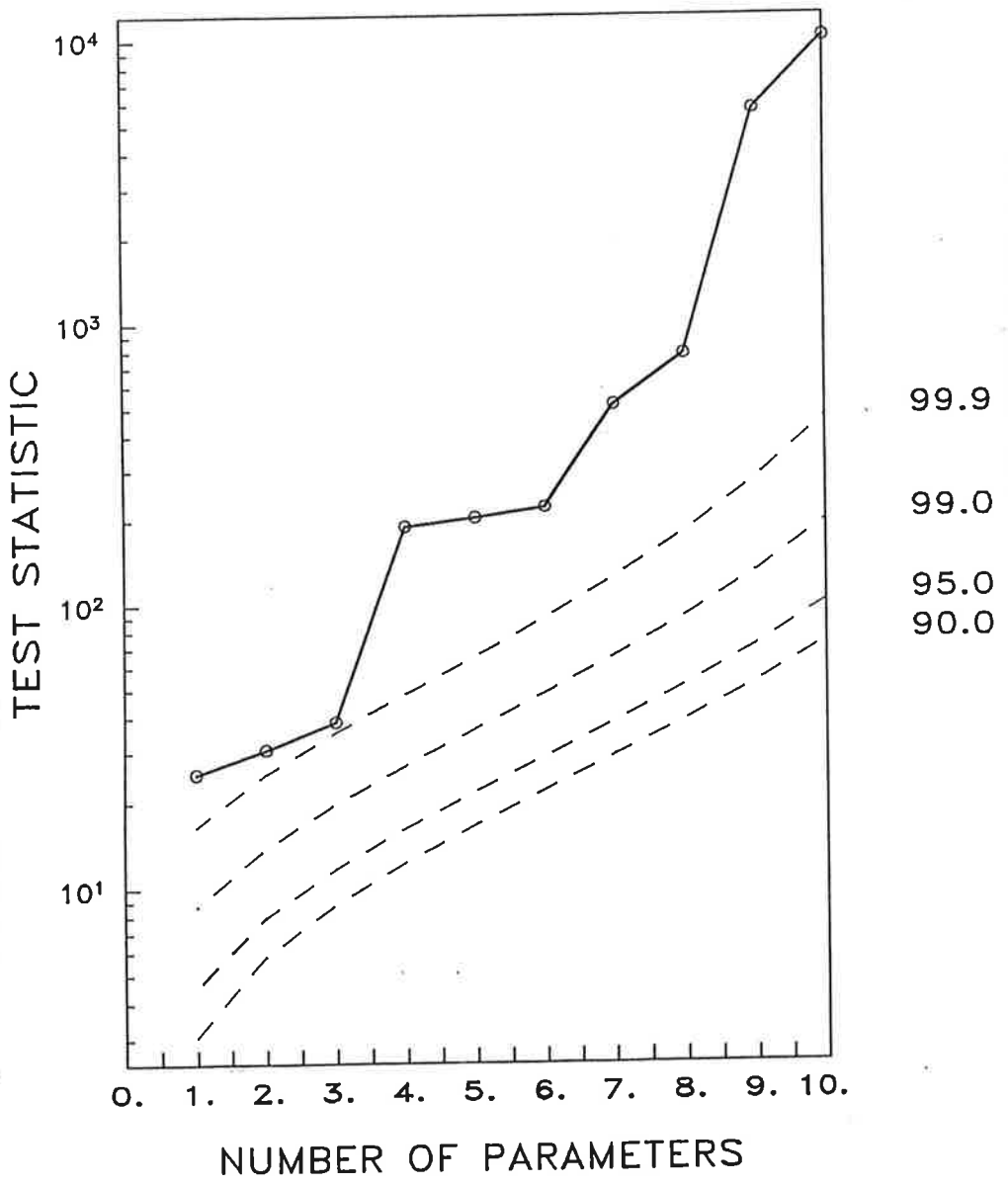

Figure 4.3: Hotelling T^2 - test of precipitation, axis see fig 4.1

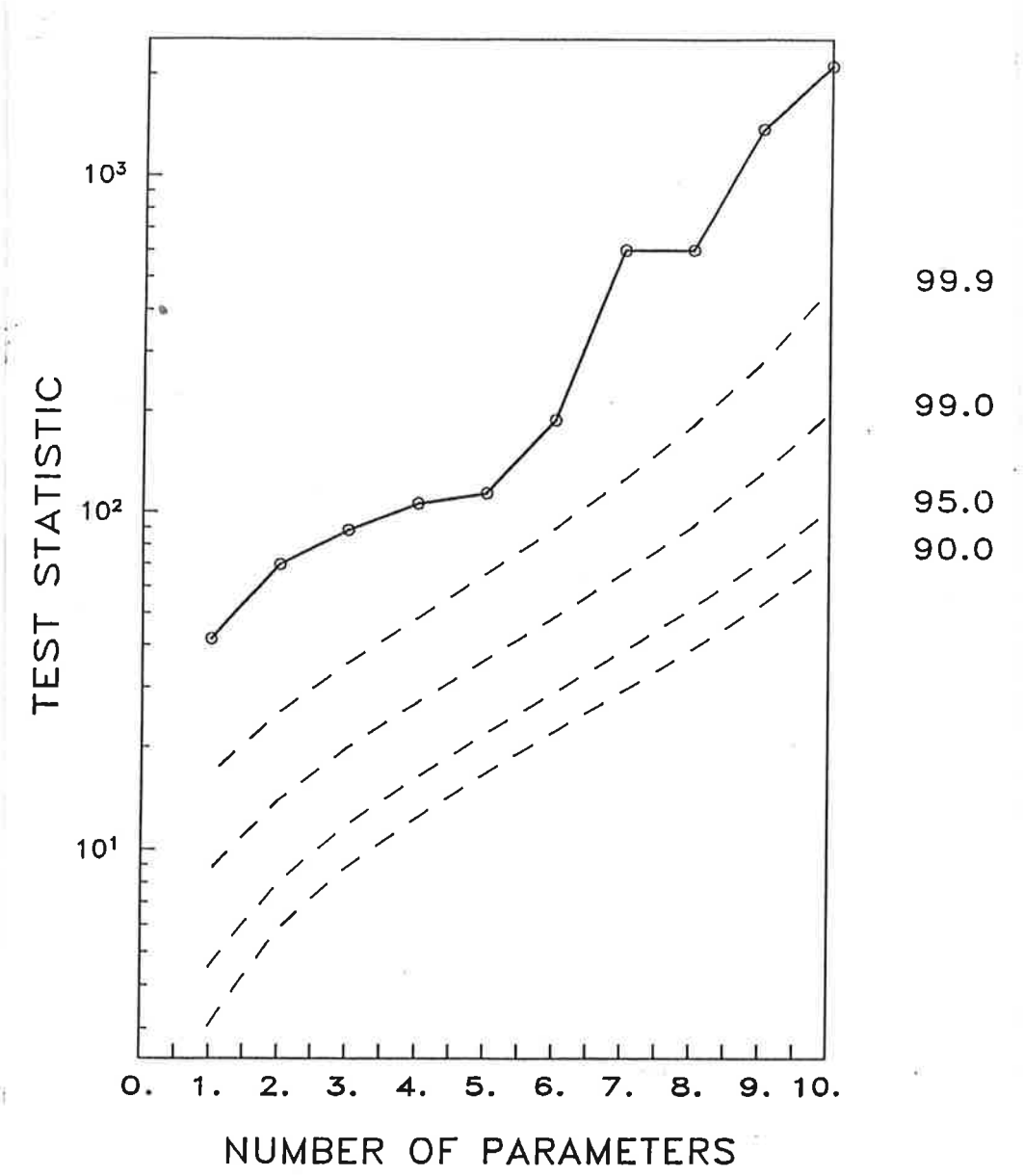

Figure 4.4: Hotelling T^2 - test of zonal surface wind, axis see fig. 4.1

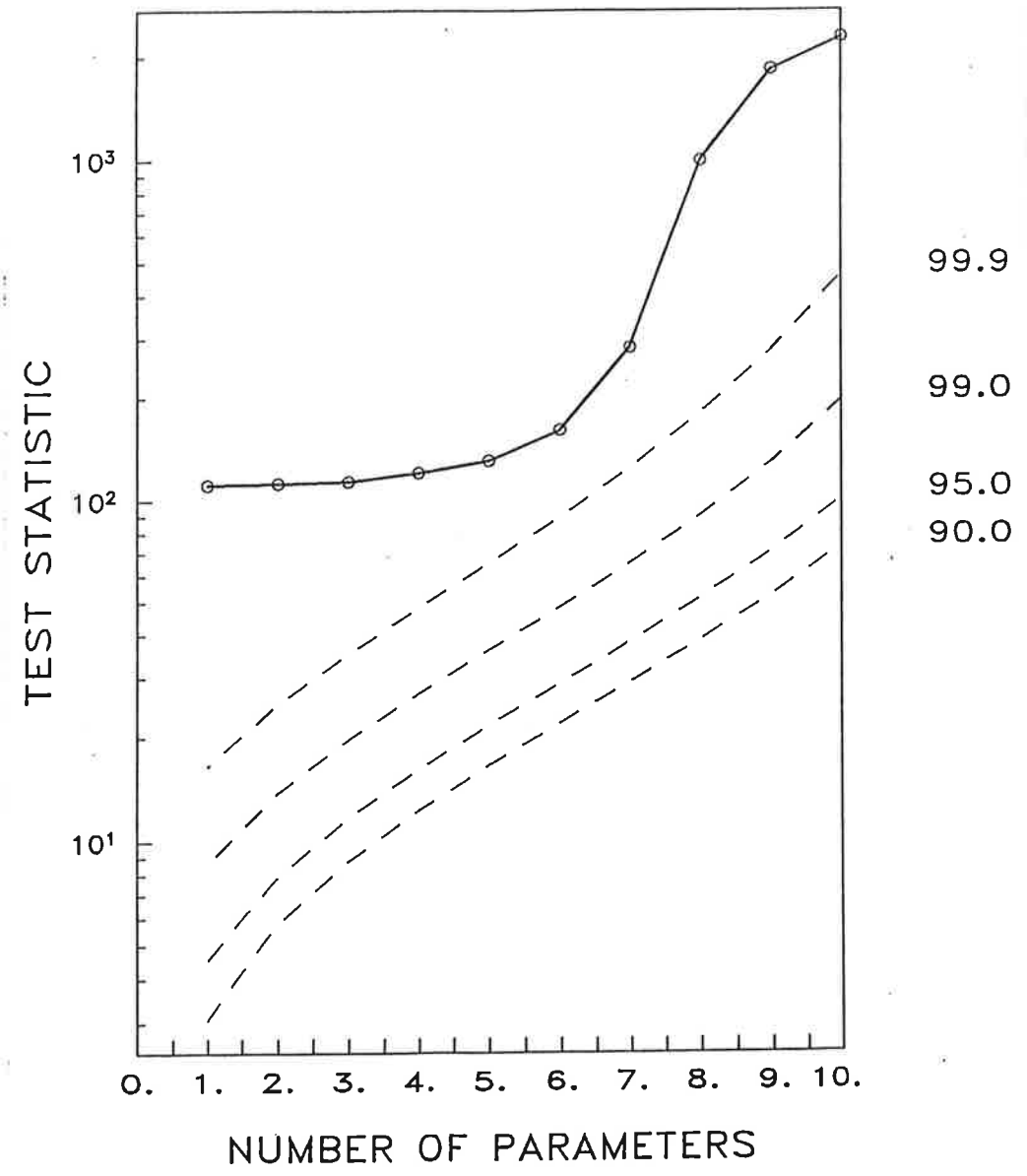

Figure 4.5: Hotelling T^2 - test of meridional surface wind, axis see fig. 4.1

5. Comparison with Observations

The control run shows a reasonable representation of the modern climate in terms of paleoclimate modelling which is evaluated by Kirk et al. (1987) and Dümenil, Schlese (1987b). The paleo-experiment reproduces the general characteristics of the ice age climate. The land surface temperature decreases in the order of 5°C - 10°C and the precipitation over land is reduced. But the general climate information -colder and drier climate 18000 YBP than today- enters the model in some sense via the deep soil boundary conditions resulting in a stabilization of the working point of the land surface relative to temperature and hydrology.

Local data for 18000 YBP resulting from core analyses of land deposits and ocean sediments are summarized below:

a) Surface wind (fig. 3.2)

Frenzel (1986) provides some information about local wind systems. In winter the wind at the west coast of India blows from land to sea which agrees with the model results. The following wind regimes are not separated seasonally. The winds from land to sea at the West-Sahara and the east of North-America agree with the model wind. The model wind direction of southeast at the coast of Mid-Europe contradicts the data, while the northern winds far away from the coast agree with the observations.

Messerli (1980) suggests that the intertropical convergence zone (ITCZ) at the west coast of Africa is shifted in January 18000 YBP from 10° north to 5° north. Looking at the model results the ITCZ seems to be slightly shifted southwards.

b) surface temperature (fig. 3.3)

Frenzel (1986) shows temperature isolines for Asia. The 0°C-line in the model agrees with the observed. The model temperatures in Central-Asia are about 10°C or more too high in comparison with Frenzel's data. The temperature increase agrees with recent results from Hövermann et al. (1986).

Frenzel (1980) suggested a reduction of temperature of about 15°C for the January climate during the last ice age in Europe. The model temperature reduction is about 10°C.

Messerli (1980) gives hints about a snow line height of 2000m in northern Africa. This glaciation corresponds partly with regions of negative surface temperature in the model.

c) precipitation (fig. 3.4)

Precipitation datas are given by Frenzel (1986) and (1967) for Asia and Northeast-Africa. The precipitation reduction is evaluated as yearly mean decrease and leads to a monthly mean reduction in the order of 20 mm which agrees with the model results.

Messerli (1980) shows the reduction of the tropical rain forests in Africa and South-America which corresponds with a precipitation decrease in the paleo-experiment

Duplessy (1982) concluds from analyse ocean sediment cores at the west coast of India that the winter monsoon in the Arabean Sea became stronger during the ice age. The enlargement of precipitation can directly be seen in the model data

The model reproduces the general state of the January climate 18000 YBP, while local features do not correspond in all details with the model results. Weighting the model results uncertaities in core data accuracy must be taken in mind.

6. Comparison with recent Simulation Results

In this section we wish to compare the T21 results of the January climate 18000 YBP with these obtained by Kutzbach, Guetter (1986) with the NCAR Community Climate Model (CCM). The atmospheric general circulation model CCM and T21 are comparable with respect to included physics and used numerical techniques. The resolution of the T21-model in grid and spectral space is a little finer as in the CCM. The boundary conditions for ice sheet location and height, sea ice extension and sea surface temperature in the CCM experiment follow the maps of CLIMAP (1981). Additional to ice and ocean surface albedo, two land surface albedo classes are specified. The modern values are locally corrected by the values of CLIMAP (1981). The CO_2-concentration is reduced from the present value of 330 ppm to 200 ppm and no aerosols are considered in the experiments of Kutzbach and Guetter. Orbital parameters determining the insolation are the same as in the T21-experiment (see sec.2).

Global fields of the quantities are available for the comparison:

a) sea level pressure	(fig. 3.1, fig. 6.1)
b) surface wind	(fig. 3.2, fig. 6.2)
c) surface temperature	(fig. 3.3, fig. 6.3)
d) precipitation	(fig. 3.4, fig. 6.4)

a) sea level pressure

Both models, CCM and T21, show the same structure of high and low pressure regions in the northern hemisphere. The maximum of the Asiatic high in the CCM is located in both runs, paleo and control, over Central-Asia. In the paleo experiment the CCM shifted the maximum to the North. The T21-model locates the maximum pressure deviation to higher values over the Himalaya.

In the southern hemisphere the high pressure regions in the control run are stronger in the CCM than in the T21-model which is a general defect in our T21-version (Kirk et al. (1987), Dümenil, Schlese (1987b)). The CCM reproduces the high pressure regions of the control run in the paleo-case but weaker, while in the paleo-run the T21-model produces low pressure regions instead of highs.

b) surface winds

In the control runs the CCM and the T21-model produce the same circulation regimes in the northern hemisphere. In the southern hemisphere the circulation produced by the models is a little different. The westerlies at latitude 40°S are stronger in the CCM than in the T21-model concerning the differences in the pressure field. The circulation over the Antarctic ice sheet is weak in the CCM while the T21-model shows stronger and more structured winds.

In the paleo-run the circulation regimes in northern hemisphere agree in both models. The control - run circulation is there modified by the North-american and the Eurasian ice sheet. In the southern hemisphere the CCM reproduces in the paleo-run the same circulation structure as in the control-experiment. The paleo-climatic circulation of the T21-model in the southern hemisphere is changed in comparison with the control run and the CCM results. The east passat in the tropical Pacific is reduced while the westerlies at 40°S and the Antarctic circulation is strengthened.

c) surface temperature

The CCM shows a land surface temperature reduction in the paleo-climate of 5° - 10°C, partly even more, in the vicinity of the ice sheets, while the

temperature changes in the tropics are negligible. Over the Antarctic region a surface temperature increase up to 5°C is obvious.

The T21-model shows a global reduction of land surface temperatures of 5°C - 10°C and even more in the vicinity of the glacial ice sheets. The temperature increase in the paleo-climate over Alaska is produced in both models, while the temperature increase over Central-Asia up to 5°C is a special feature of the T21-model.

d) precipitation

A general precipitation reduction in the paleo-climate over land in the tropics is not obvious in the CCM results, but is realized in the T21-climate. The increase of winter monsoon during the last ice age in the Indian area is in the CCM not as clear as in the T21-model. The precipitation increase in the eastern tropoical Pacific is not realized in the CCM paleo experiment.

The CCM produces only local circulation changes in the vicinity of the ice sheets for the paleo-climate. The paleo-climate of the T21-model shows global circulation changes especially in the southern hemisphere. At this time it cannot be decided whether the circulation patterns of the T21-model or the wind distribution of the CCM is closer to the paleo-climate because of the lack of observed circulation data. The tendency of the CCM producing local changes instead of global ones is also visible in the global temperature and precipitation distribution.

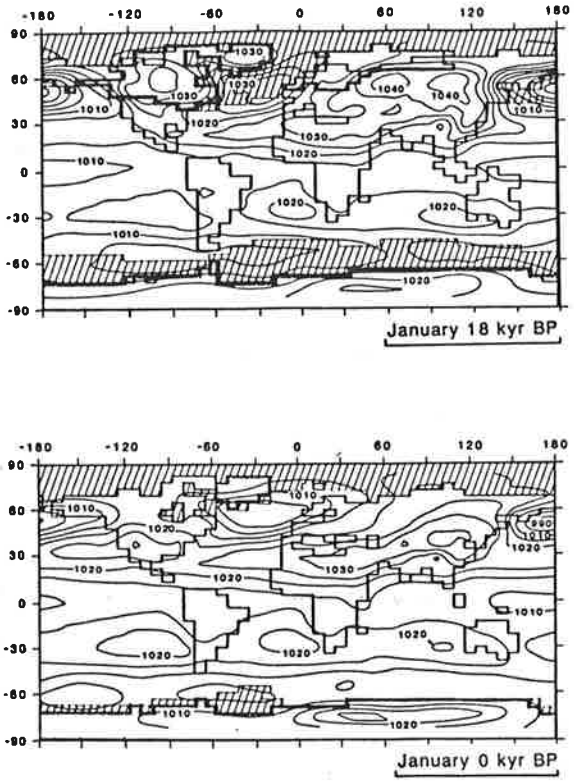

Figure 6.1: Sea level pressure, units: HPA(Kutzbach, Guetter (1986))

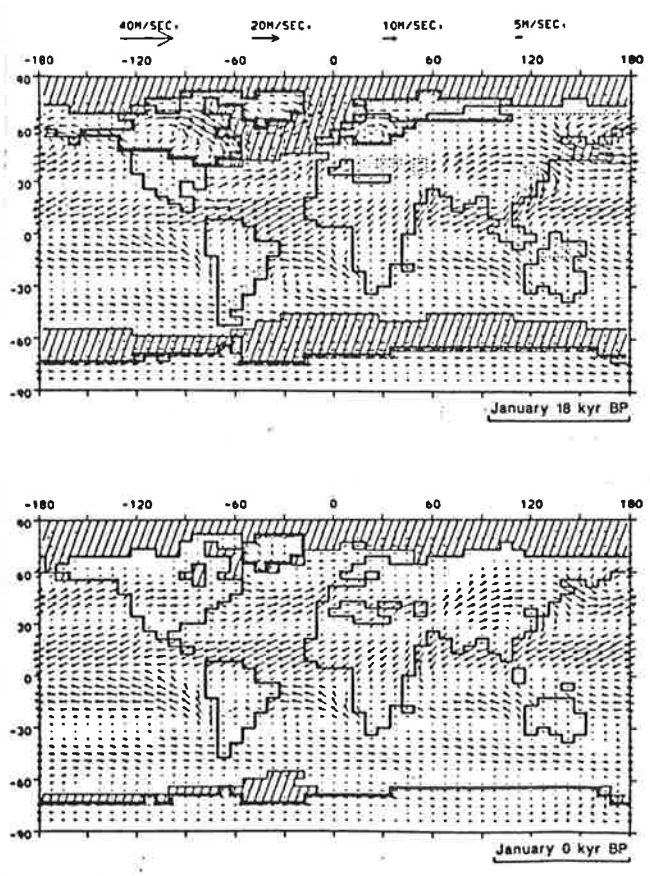

Figure 6.2: Surface winds (Kutzbach, Guetter ((1986))

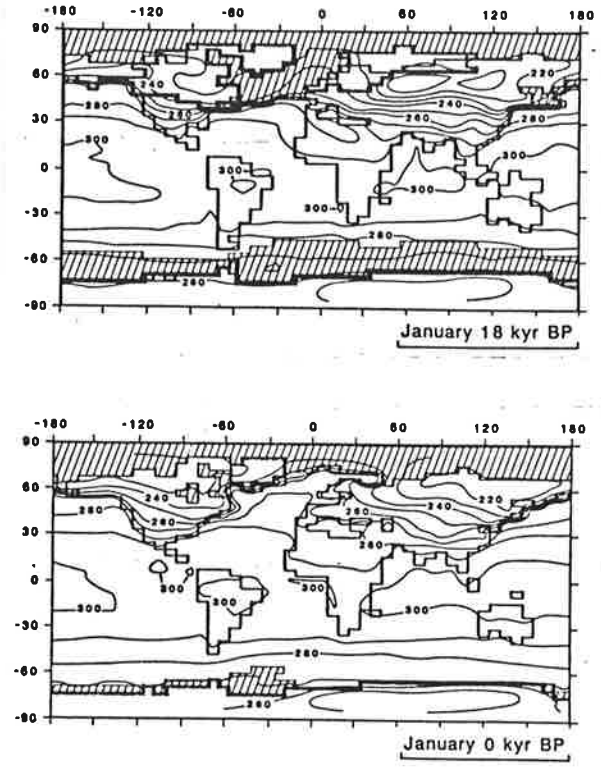

Figure 6.3: Surface temperatures, units: °K (Kutzbach, Guetter (1986))

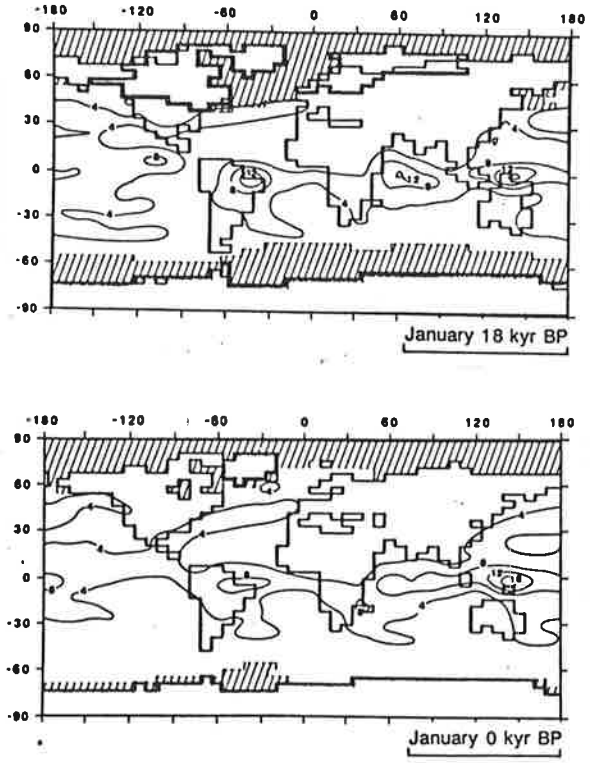

Figure 6.4: Precipitation, units: mm / day (Kutzbach, Guetter (1986))

7. Conclusions

The January climate 18000 YBP simulated with the T21-model agrees mostly with the known climatic ice age features. The atmospheric GCM responds to the ice age boundary conditions with statistically significant global changes in the paleo-climate compared to the present climate state. The month-to-month variabilities at 18000 YBP and at 0 YBP are of the same order of magnitude in the model. The glaciation of the Himalaya seems to be important in the paleo - climate.

The work will be continued by an extention of the signal-to-noise analysis to global fields of variables in the upper atmosphere and an univariate consideration of the single test pattern to identify regions with large significant differences between the paleo and the present climate state. A paleo-climate anomaly-run is planned with no glaciation of the Himalaya to analyse in more detail the influence of the Himalaya on the climate state. The numerical experiments will be continued by the simulation of the 18000 YBP annual cycle. The presented experiments concerning the January climate 18000 YBP and 0 YBP will be evaluated with regard to atmospheric circulation details and atmospheric energetics.

Acknowledgements

The authors are greatly indebted to the climatic research group of Prof. K. Hasselmann and the large scale atmospheric modelling group of Prof. G. Fischer for helpful discussions and software support during the experiments. Setting up the statistic program 'SNAP' by Dr. T. Bruns is also acknowledged.

References

Abramowitz, M., Stegun, A. (1968): Handbook of mathematical functions; Dover Publications, Inc., New York.

CLIMAP Project Members, 1981: Seasonal reconstructions of the earth's surface at the last glacial maximum; Geol. Soc. Amer. Map Chart. Ser., MC-36.

CLIMAP Project Members, 1976: The surface of the ice-age earth; Science 191, 1131-1136.

Diercke, C., Dehmel, R., 1968: Diercke Weltatlas; Georg Westermann Verlag, Braunschweig.

Dümenil, L., Schlese, U. 1987a: Description of the general circulation model; from: Climate simulalations with the ECMWF T21-model in Hamburg, Ed.: G. Fischer, Meteor. Inst. Large Scale Atmosph. Model . Rep. No. 1.

Dümenil, L., Schlese, U., 1987b: Changes in the parameterization package and their impact on perpetual January simulations; from: Climate simulations with the ECMWF T21- model in Hamburg, Ed.: G. Fischer, Meteor. Inst. Large Scale Atmosph. Model. Rep. No. 1.

Dupplessy, J.C., 1982: Glacial to interglacial contrasts in the northern Indian ocean; Nature 295, 494-497.

Frenzel, B., 1986: Maps of wind, temperature and precipitation data, private communication with K. Herterich.

Frenzel, B., 1980: Das Klima der letzten Eiszeit in Europa; from: Das Klima - Analysen und Modelle, Geschichte und Zukunft, Ed.: K. Oeschger., B. Messerli, M. Svilar, Springer -Verlag, Berlin-Heidelberg.

Frenzel, B. 1967: Die Klimaschwankungen des Eiszeitalters; Vieweg + Sohn, Braunschweig.

Hannoschöck, G.,C. Frankignoul, 1985: Multivariate statistical analysis of a sea

surface temperature anomaly experiment with the GISS general circulation model I; Journ. Atmosph. Sci., 42,13, 1430-1450.

Hannoschöck, G., 1984: A multivariate signal-to-noise analysis of the response of an atmospheric circulation model to sea surface temperature anomalies (Dissert.); Hamburger Geophysikalische Einzelschriften, Reihe A, Heft 67.

Hövermann, J., Süßenberger, H., 1986: Zur Klimageschichte Hoch-und Ostasiens, Berliner Geograph.Studien 20, 173-186.

Kirk, E. ,M., Ponater, A. Kirk, 1987: Circulation statistics of the T21-GCM; from: Climate simulations with the ECMWF T21-model in Hamburg, Ed..G. Fischer, Meteor. Inst. Large Scale Atmospher. Model. Rep. No. 1, (in press).

Kuhle, M., 1986: Die Vergletscherung Tibets und die Entstehung von Eiszeiten; Spektrum der Wissenschaft Heft 9, 86, 42-54.

Kutzbach, J.E, P.J. Guentter, 1986: The influence of changing orbital parameters and surface boundary conditions on climate simulations for the past 18000 years; Journ. Atmosph. Sci. 43,16, 1726-1759.

Louis, J.-F., 1984: ECMWF forecast model: physical parameterization; ECMWF Research Department, Research Manual 3.

Messerli, B., 1980: Die afrikansischen Hochgebirge und die Klimageschichte Afrikas in den letzten 20000 Jahren, from: Das Klima - Analysen und Modelle, Geschichte und Zukunft, Ed.: H. Oeschger, B. Messerli, M. Svilar, Springer-Verlag, Berlin-Heidelberg.

Rotta, J.C., 1972: Turbulente Strömungen, B. G. Teubner, Stuttgart.